Journal of Materials Chemistry A

Accepted Manuscript

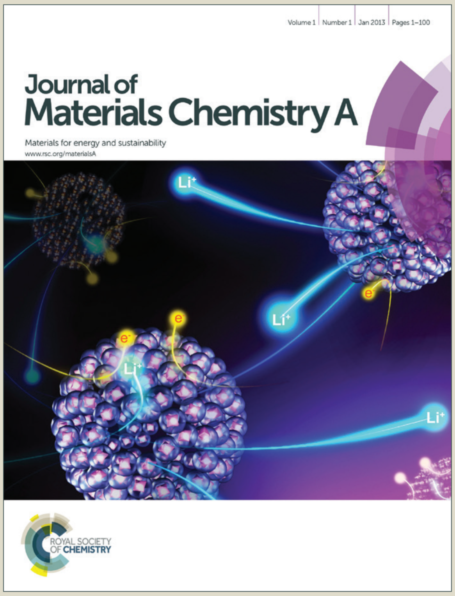

ROYAL SOCIETY OF CHEMISTRY

www.rsc.org/materialsA

Table of Contents Graphic

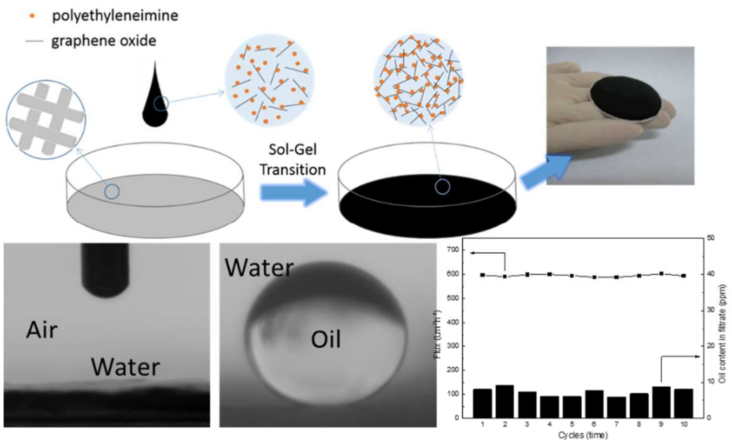

A non-laminated graphene oxide membrane with superhydrophilic and underwater superoleophobic properties was fabricated by sol-gel process for effective oil/water separation.

Journal Name

ARTICLE

Sol-Gel Fabrication of a Non-Laminated Graphene Oxide Membrane for Oil/Water Separation

Received 00th January 20xx,
Accepted 00th January 20xx

DOI: 10.1039/x0xx00000x

www.rsc.org/

Tiefan Huang,[a] Lin Zhang,*[a] Huanlin Chen,[a] Congjie Gao[a,b]

A non-laminated graphene oxide membrane crosslinked by polyethyleneimine was prepared via a one-step sol-gel process. In the as-prepared membrane, the GO nanosheets remain disordered as in the sol state to form a randomly arranged GO assembly structure, which results in a much higher flux compared with the general laminated GO membrane prepared via vacuum filtration or spin coating because of the lower flow resistance. Further, this random assembly of GO nanosheets give rise to a hierarchical micro/nanoscale rough structure on the membrane surface. Along with the crosslinking reaction, PEI was grafted onto the GO nanosheets to make them hydrophilic. Combining the hydrophilic surface chemistry with the micro/nanoscale hierarchical surface structure, the non-laminated GO membrane exhibited the desired superhydrophilic and underwater superoleophobic properties. We have tested the membrane to separate a series of surfactant-free and surfactant-stabilized oil-in-water emulsions. A high separation efficiency (>99%) and flux were achieved using only gravity without any extra power, much larger than commerical filtration membranes with similar permeation properties. Moreover, the membrane shows an outstanding antifouling performance for oil droplets and can be recycled easily for long-term use.

Introduction

Graphene oxide (GO), which is an oxidative derivative of graphene, bears many oxygen functional groups on its basal planes and edges, and the chemical structure endows GO with excellent hydrophilicity and dispersity in many solvents.[1] This improved processing property compared to graphene makes GO a suitable building block to construct various macro-assemblies.[2-9] In particular, because of their excellent membrane formation characteristics, GO membranes have been widely studied in many fields.[10-15]

Previous reports in the literature on membrane-related applications of GO have focused on its laminated micro-structure. GO membranes with laminated microstructures are prepared by a filtration-assisted assembly or spin-coating method.[16, 17] Using wrinkled hydrazine reduced GO, Li et al. fabricated a wet graphene membrane via vacuum filtration and investigated its application in nanofiltration for nanoparticles and dyes.[18] Geim et al. constructed a micrometer-thick GO membrane via the spin-coating method, which showed unimpeded evaporation of water but was completely impermeable to liquids, vapors, and gases (even helium).[19] Gao et al. fabricated an ultrathin graphene membrane using base-refluxing reduced GO, which showed high retention rates for organic dyes and moderate retention rates for salts.[20] Very recently, Jin et al. prepared a GO membrane supported on a ceramic hollow fibre membrane for the pervaporation separation of dimethyl carbonate/water mixtures.[21] In these GO membranes, GO nanosheets tend to be in horizontally aligned stacks and form well-ordered laminated microstructures. This face-to-face arrangement of the GO nanosheets was proposed as a result of van der Waals attractions, π-π interactions and hydrogen bonding between adjacent nanosheets, as observed in the dried graphene paper and theoretical simulation.[22, 23] To strengthen the bond between adjacent GO nanosheets to improve GO membrane stability in water, crosslinking between laminated microstructure was also studied.[24-29]

The nanocapillaries formed between adjacent GO nanosheets in laminated membranes provide a diffusion route for molecule permeation. Because the nanocapillaries are vertical to the apparent permeation orientation, the molecular diffusion route is unexpectedly long.[19] Therefore, although the laminated microstructure has many advantages, such as a molecular-sieving function, it inevitably makes the flow resistance significantly large, resulting in a low flux that fails to meet expectations. Under some circumstances, such as ultrafiltration, high flux is needed, which laminated GO membranes cannot satisfy. Further, on the laminated

---

[a] *Key Laboratory of Biomass Chemical Engineering of MOE, Department of Chemicaland Biological Engineering, Zhejiang University, Hangzhou 310027, China. E-mail: linzhang@zju.edu.cn; Fax: +86-571-87952121; Tel: +86-571-87953802*

[b] *College of Ocean, Zhejiang University of Technology, Hangzhou 310014, China*

† Electronic Supplementary Information (ESI) available: Porosity calculation, separation apparatus, high magnification top view SEM images of LGM, sliding angle measurement of 1,2-dichloroethane (DCE) droplets on the NLGM in water, separation results for other emulsion systems, SEM images of the NLGM after oil/water emulsion separation performance test, photograph of an underwater oil droplet on the NLGM and simulated underwater drag deformation force tests after oil/water emulsion separation test and element component percentages of GO and the NLGM, and. See DOI: 10.1039/x0xx00000x†

membrane surface, GO nanosheets are horizontally aligned, the membrane surface morphology is rather smooth and there is a lack of obvious structure characteristics, which may be important for possessing superwetting properties.[30-36]

In this work, we report a kind of novel GO membrane with a non-laminated microstructure that is completely different from previous GO membranes reported. Herein, the GO membrane was prepared via a one-step sol-gel process using polyethyleneimine (PEI) as the crosslinker to produce randomly assembled GO nanosheets in the membrane rather than laminated stacked, forming a non-laminated microstructure. Therefore, the non-laminated membrane with more pore space has a much higher flux. Further, in the non-laminated membrane, the randomly arranged graphene oxide assembly gives rise to a micro/nanoscale hierarchical structure on the membrane surface to endow the membrane with superhydrophilic and underwater superoleophobic properties. The non-laminated GO membrane can separate a series of surfactant-free and surfactant-stabilized oil-in-water emulsions driven solely by gravity without any extra power with a high separation efficiency (water purity in the filtrate after one-time separation > 99 wt %) and a relatively high flux. Most importantly, due to the ultralow affinity of its surface to oil drops, the non-laminated membrane exhibits excellent antifouling properties, which make it practical for long-term recycled use.

Experimental

Chemicals and Materials

Graphene oxide (GO), prepared using a modified Hummers method from flake graphite, was manufactured by XFNANO Material Tech Co. (Nanjing, China). Branched polyethyleneimine (PEI) with a molecular weight of 10,000 was purchased from Sigma-Aldrich (St. Louis, USA). Non-woven fabric was purchased from Paper Group (Fremont, USA). Isopar G was purchased from Exxon Mobil Co. (Irving, USA). All other chemicals were obtained from Sinopharm Chemical Reagent Co. (Shanghai, China). The deionized water (electrical resistivity>17 MΩ•cm) used throughout the experimental process was produced in our laboratory.

Preparation of the Non-laminated GO Membrane (NLGM)

The NLGM was prepared using a facile sol-gel process. In brief, GO powder (16 mg) was dispersed in water (2 ml) and ultrasonicated for 1.5 h. Then, a NaOH aqueous solution (4 M) was added to the dispersion until the pH=12.8. A PEI aqueous solution (16 mg/ml, 0.25 ml) was then added and vigorously stirred, and the resulting sol was slowly drop-cast on non-woven fabric. The final NLGM was obtained by a sol-gel process, which was performed in a sealed pot at 80°C for 8 h. Before the characterization or separation processes, the membranes were rinsed by filtering copious amounts of water to remove physically adsorbed PEI and residual NaOH. The laminated GO membrane (LGM) was prepared by a vacuum filtration method as a control, using GO (8 mg) and a PEI aqueous solution (16 mg/ml, 0.125 ml).

Preparation of the Oil-in-water Emulsion

Surfactant-free oil-in-water emulsions were prepared by mixing water and oil (hexane, octane, toluene and Isopar G) at 99:1 (v/v), and the mixtures were sonicated under a power of 2 kW for 2 h to obtain homogeneous and white emulsions (hexane/water (H/W), octane/water (O/W), toluene/water (T/W) and isopar G/water (I/G) emulsions). The droplet sizes of the emulsions were in the range of hundreds of nanometers to several micrometers, as determined by optical microscopy observation. Surfactant-stabilized oil-in-water emulsions (Tween80-stabilized toluene/water (T80/T/W), SDS-stabilized octane/water (S/O/W) and SDS-stabilized isopar G/water (S/I/W)) were prepared by adding surfactant (SDS or Tween80) via similar process. The surfactants concentration in these emulsion was about 0.02mg/ml. These emulsions are stable at least for 12h without obvious demulsification occurred. The droplet sizes are in the range of several hundreds of nanometer to 2 µm.

Emulsion Separation Experiment

Oil-in-water emulsion separation experiments were performed driven by gravity and the separation apparatus is shown in Figure S1. The prepared emulsion of 150 ml was poured onto the NLGM and spontaneously permeated quickly. The flux was determined by counting the time to produce 10 ml of permeate using the following equation: Flux=10 ml/At, where A is the valid area of the membrane (12.56 cm^2) and t is the testing time. For each test, three samples were measured to obtain the average value.

Instruments and Characterization

Fourier transform infrared (FTIR) spectra were recorded on a Bruker Tensor27 spectrometer. The samples were prepared as KBr pellets, and the spectra were calculated from a total of 32 scans. X-ray diffraction (XRD) was carried out using an X'Pert PRO (PANalytical, Netherland) X-ray diffractometer with Cu KR radiation (λ = 1.5406 Å). Scanning electron microscopy (SEM) images were obtained on a field-emission scanning electron microscope (Hitachi SU8010, Japan). Contact angle measurements were conducted on the drop shape analysis system DIGIDROP-DI (GBX Co, France). X-ray photoelectron spectroscopy (XPS) was performed on an Axis-Ultra DLD spectrometer (Kratos Co, USA) using Al Kα radiation at a base pressure of 3 × 10^{-9} mbar, and the binding energies were referenced to the C1s line at 284.5 eV from adventitious carbon. Thermogravimetric Analysis (TGA) was performed on TA-Q500 (TA Co. USA) with temperature increase of 10°C/min under nitrogen environment. Optical microscopy images were taken with a CFM-330 microscope (Changfang Optic Inc., China) equipped with D60 (Nikon, Japan) by dropping the solution on a biological counting board. Total organic carbon (TOC) was determined using a TOC meter (Liqui TOC, Elementar Analysensysteme GmbH). The tests were repeated three times and the results given were the average values.

Results and Discussion

Preparation and Characterization of NLGM

As shown in Figure 1a, the NLGMs were fabricated by a one-step sol-gel process, wherein PEI served as the chemical crosslinker and a non-woven fabric was used as the substrate. In the sol state, the reaction between PEI and GO is insufficient, so almost all of the GO nanosheets in solution were free. During heating treatment, sol-gel inversion occurred: PEI crosslinked free GO nanosheets in the sol, constructing a 3D network structure of the membrane, in which GO nanosheets maintained their random orientation as in the sol.

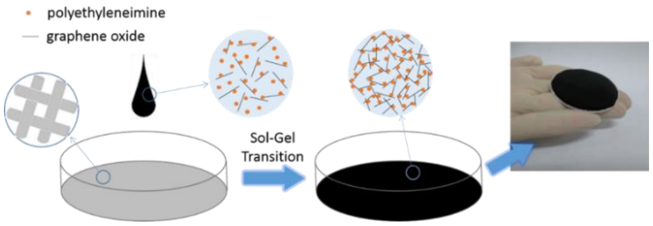

Figure 1. Schematic illustration of the formation of an NLGM via the sol-gel process.

The successful crosslinking reaction of GO by PEI was confirmed by FTIR spectroscopy and XPS. Compared with the FTIR spectrum of GO (curve I, Figure 2), an increase in the peak intensity at 1114 cm^{-1}, which corresponds to the stretching vibration of the new C-N bonds and the residual group of PEI, was observed in the NLGM (curve II, Figure 2). The peak intensity of the NLGM at 2930 cm^{-1} and 2845 cm^{-1} (inset in Figure 2), which corresponds to the C-H stretching vibrations of PEI (curve III, Figure 2), substantially increased. The peak in the region corresponding to the -COOH stretching vibration at 1726 cm^{-1} decreased, which is attributed to the possible electrostatic interaction between GO and PEI.[37] In addition, a peak appeared at 1578 cm^{-1}, and this peak corresponds to the unoxidized aromatic domain of GO. This result demonstrates that PEI reduced GO to some extent along with the crosslinking reaction.[38]

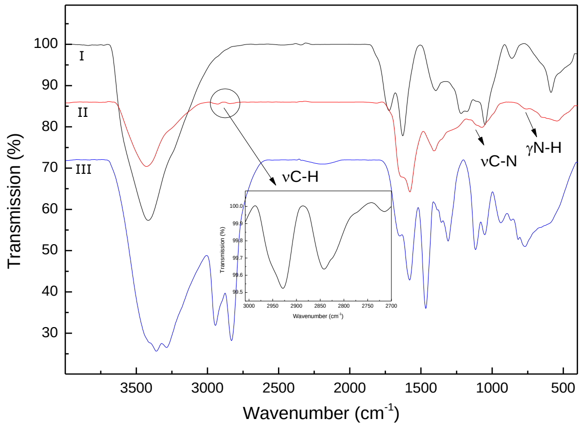

Figure 2. FTIR spectra of GO (I), NLGM (II) and PEI (III)

Figure 3a presents the survey XPS spectra of GO and the NLGM; the element component percentages of GO and the NLGM are displayed in Table S1. For the NLGM spectra, due to reaction with PEI, an obvious peak at 396.4 eV was observed, which can be attributed to the N1s binding energy, whereas only a tiny peak in this position was observed for GO, which was probably introduced during the preparation of GO. To further discuss the elemental analyses of the composite membranes, the C 1s region of the XPS spectra was deconvoluted. As shown in Figure 3b, the unmodified composite membrane shows curve fittings with five peaks representing different component species: C-C/C=C, C-OH, C-O-C, C=O and O-C=O, when the binding energy was 284.5, 285.1, 286.4, 287.3, and 288.5 eV, respectively.[39] After treatment of PEI, some of the peak component intensities were reduced, indicating that GO was partially reduced by PEI, which is consistent with FTIR results. In addition, there is a predominant peak component at approximately 286 eV, corresponding to the C–N component, suggesting that PEI successfully reacted with GO.[40] For convenient comparison, the percentages of each carbon component (excluding C-N) calculated from the peak area integral for the GO membrane and NLGM are listed in Table 1. After reacting with PEI, the C-O-C and C-OH peak intensities of the NLGM changed in an opposite trend: the peak intensity of the C-O-C showed a substantial decline, whereas that of the C-OH peak increased. These observations suggest a nucleophilic substitution reaction, in which an amine of the PEI attacks the carbon atom of the epoxy group of GO; therefore, the three-membered epoxide ring was opened, resulting in C-N and C-OH groups.[28] In this reaction, we infer that PEI not only crosslinked individual GO nanosheets together, integrating the membrane, but also grafted on the GO nanosheets, making it more hydrophilic.

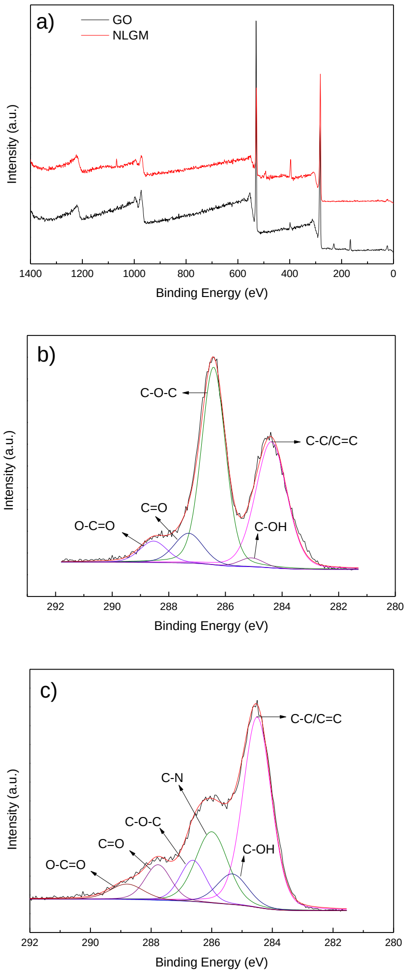

Figure 3. a) Survey XPS spectra and b-c) C1s XPS spectra of the GO and NLGM, respectively.

Table 1. C1s Component Peak Areas as the Percentages of the Total Area of the GO and NLGM

	C-C/C=C [%]	C-OH [%]	C-O-C [%]	C=O [%]	O-C=O [%]
GO	38.1	2.08	45.8	8.30	5.71
NLGM	61.1	10.7	12.0	10.3	5.8

In order to determine the amount of PEI in the NLGM, TGA measurement was carried out, as shown in Figure 4. GO was thermally unstable and starts to lose mass upon heating even below 100°C, with a moderate weight loss that resulted from the removal of adsorbed water. Starting from 140°C, a rapid weight loss was observed, attributable to the removal of labile oxygen-containing functional groups. The PEI showed a rapid weight loss between 325°C and 410°C. As to the curve of NLGM, compared with that of GO and PEI, its decomposition curve showed the combination of both of them. The weight loss region from 290°C to 410°C could be attributed to the decomposition of PEI with a weight loss of 19.8%, indicating that almost all PEI was reacted for GO nanosheets crosslinking in the sol-gel process. Since the GO was partially reduced by PEI as well, the removal of thermally labile oxygen functional groups resulted in the much increased thermal stability for the reduced GO, which makes the NLGM had lower weight loss than that of GO.[41,42]

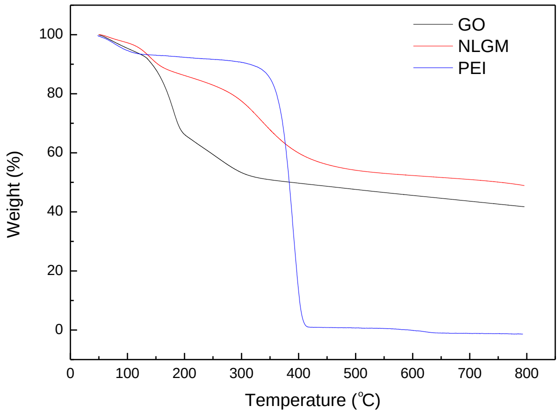

Figure 4. TGA of GO, PEI and NLGM.

Due to PEI cross-linking, the mechanic stability of the membrane was significantly improved. In order to prove this, we prepared NLGM without PEI crosslinking, via similar preparation method, as a control. Figure 5 shows the NLGMs with and without PEI crosslinking after oscillation (60 rpm) for 1h and 1 day in water, respectively. During the oscillation process, the NLGM without PEI crosslinking disintegrated rapidly, which resulted in the water becoming yellow brown. In contrast, the integrity of the NLGM with PEI crosslinking was maintained after oscillation period as long as 1 day, and the water still remained clear and clean, which indicated that the NLGM stability significantly improved due to PEI crosslinking. This ensured the potential of the membrane for practical application.

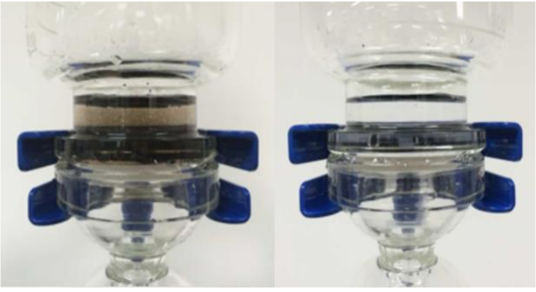

Figure 5. Photographic images of the NLGMs with (right) and without (left) PEI crosslinking after oscillation (60 rpm) for 1h and 1 day in water, respectively.

Effect of the Sol-Gel Process on the Membrane Microstructure

The XRD spectra of the NLGM are given in Figure 6, and the LGM is also displayed. For the LGM prepared by vacuum filtration, an intensive peak was observed at 2θ = 9.62°. This indicates an ordered arrangement of GO nanosheets in the membrane, similar to previous related reports.[28, 29] However, no obvious peaks appear in the NLGM, which demonstrates that, as we anticipated, the GO nanosheets in the NLGM were completely separated as in the sol state and remained in a rather disorder arrangement after the crosslinking reaction during the sol-gel process.[43-45]

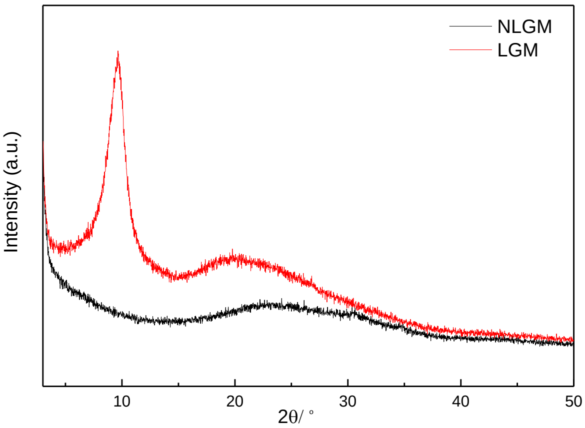

Figure 6. XRD patterns of the NLGM and LGM.

Scanning electron microscopy (SEM) images of the NLGM and LGM at different magnifications are given in Figure 7. From the cross-section view, it is obvious that the NLGM exhibits a homogeneous sponge-like structure with a thickness of 250 μm (Figure 7a), which is much thicker than that of the LGM prepared via the vacuum filtration method (Figure 7b) because most GO nanosheets in the NLGM were not stacked horizontally but in random arrangements. The structure of the NLGM is characterized by interconnected pores, and these pores may form numerous tortuous and continuous passageways for liquid to flow. From the top view, the surface of the NLGM is composed of numerous GO nanosheet clusters on the micrometer scale (circled in Figure 7d for instance). These clusters are connected with each other but are disorderly arranged, which makes the membrane surface rather rough. On the surfaces of these clusters, finer protrusion structures on the nanometer scale (circled in Figure 7e for instance) are clearly recognized. These clusters and finer protrusion structure were originated from the twisted GO nanosheets, which is caused by the high reaction temperature and high pH value condition during the sol-gel process.[46, 47] The crosslinking effect of PEI also can make the GO nanosheets corrugated, because PEI molecules would be unrestricted in reaction at either termini with different sites of the graphene sheet, potentially leading to intrasheet bonding, induced curvature and folding.[48] In contrast, this micro/nanoscale hierarchical structure is not observed on the surface of the LGM prepared by the filtration method; its surface is fairly smooth with only slight waves, as shown in Figure 7f. (Figure S2 for higher magnification). The porosity of the NLGM can be calculated from materials density[49] and membrane thinkness perspectives, and the two calculated porosities, nearly the same, are 97.4% and 98.4%, respectively (see supporting information), which are similar to other reports of GO-based hydrogel.[50-53]

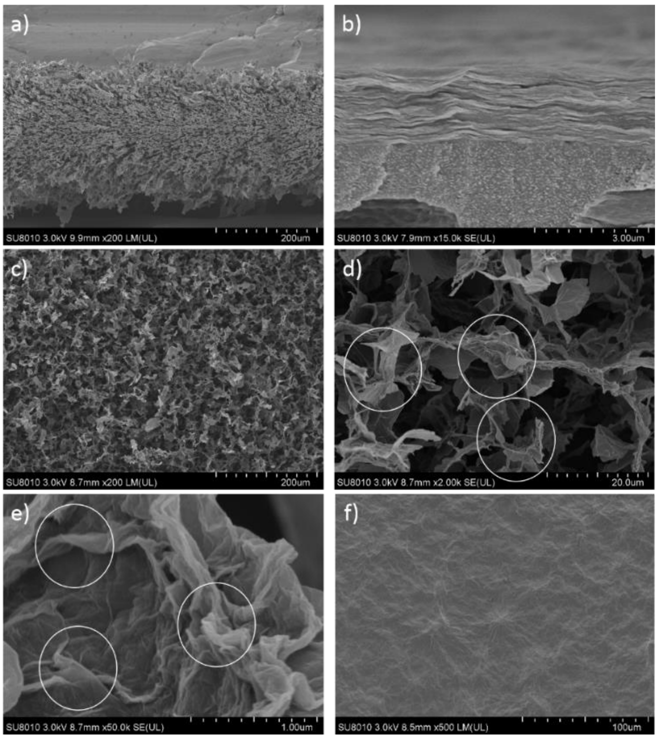

Figure 7. Cross-section view of the NLGM (a) and the LGM (b); top view SEM images of the NLGM (c-e) and the LGM (f).

Effect of the Membrane Surface Microstructure on the Underwater Superoleophobic Property

We examined the wetting behavior of oil and water on the top surface of the NLGM, as shown in Figure 8. A water contact angle (CA) of approximately 0° in air and an underwater oil (1,2-dichloroethane is taken as an example) contact angle (OCA) of approximately 160° are observed, suggesting superhydrophilic and underwater superoleophobic properties. As a control, the OCA of the LGM was 143°, less than the common standard superwetting property (Figure 8b).[54] Because the two types of membrane have the same surface chemistry, this wetting difference can be attributed to the surface microstructure distinction. According to the Cassie-Baxter theory, the micro/nanoscale hierarchical structure is important for materials possessing superwetting properties.[55] Combined with the hydrophilic PEI-grafting GO nanosheets, the NLGM exhibited superhydrophilic and underwater superoleophobic properties. In water, the NLGM contained water in its balanced state. When an oil droplet contacts the membrane surface, water can be trapped in the rough micro/nanoscale structures and forms an oil/water/solid composite interface, showing excellent underwater superoleophobic properties. These trapped water molecules greatly decrease the contact area between the oil droplet and the solid surface. Hence, these results clearly demonstrated that the micro/nanoscale hierarchical structure is essential for membranes to have superwetting properties. The oil-droplet sliding angle of the NLGM in water was found to be about 2.2° as shown in Figure S3.

To further characterize the dynamic wetting behavior of oil on the NLGM surface, simulated underwater drag deformation force tests of oil-droplets were performed, as demonstrated in Figure 8c. A droplet was squeezed to sufficiently contact the membrane surface with an obvious deformation, and it was then lifted up. There is no deformation observed during the leaving process, thus indicating extremely weak oil affinity to the membrane surface.

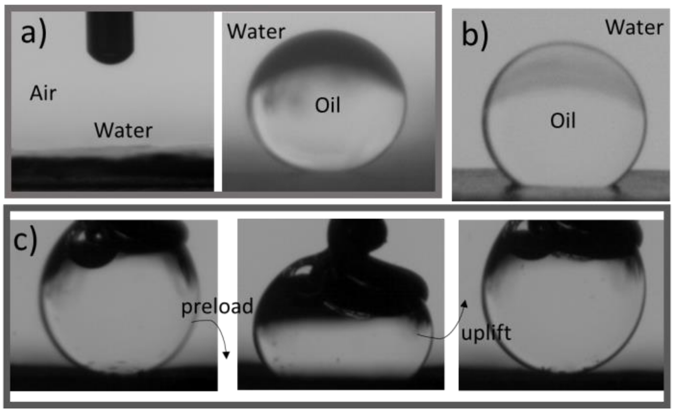

Figure 8. a) Photographs of a water droplet and an underwater oil droplet on the NLGM, respectively. b) Photograph of an underwater oil droplet on the LGM. c) Photographs of the simulated underwater drag deformation force tests of an oil-droplet on the NLGM.

Separation Performance of the NLGM for Oil/Water Emulsions

Based on the superhydrophilic and underwater superoleophobic properties, we have applied the NLGM for oil/water emulsion separation. Usually, in practical industry separation processes, water has a higher density than oils; hence, the superhydrophilic and underwater superoleophobic properties of the NLGM would form the water-layer on the membrane surface and avoid direct contact between oil-droplets and membrane surfaces. It could greatly alleviate the membrane fouling phenomenon and maintain a high separation efficiency with time. To test the oil/water separation performance of the NLGM, both surfactant-free oil-in-water emulsions (T/W, H/W, O/W and I/G) and surfactant-stabilized oil-in-water emulsions (T80/T/W, S/O/W and S/I/W) were prepared. The as-prepared emulsions were then poured onto NLGMs to perform filtration separation. The whole process is driven solely by gravity. The collected filtrate (right) is totally transparent compared to the original milky white feed emulsion (left), as shown in Figure 9a and Figure 9b, which takes the toluene/water emulsion and Tween80-stabilized toluene/water as an example. Under optical microscopy, it can be seen that in the feed solution, numerous oil droplets with sizes from hundreds of nanometers to several micrometers flood the entire view, whereas no oil droplets were observed in the collected filtrate, indicating the effectiveness of the NLGMs for separating various toluene/water emulsions. Similar effective separation are also achieved for other oil/water systems (Figure S4). The precise oil content in the filtrate was measured by a total organic carbon (TOC) analyzer. As shown in Figure 9c, for various oil/water emulsions, including hexane, octane and isopar G, the oil contents after separation were almost less than 10 ppm, which suggested a high separation efficiency (>99.5%) of the membrane, which can be attributed to its superhydrophilicand underwater super oil-repelling properties. Unlike the three other aliphatic hydrocarbons that are nearly insoluble in water, the oil content in the filtrate after separation of the toluene/water emulsion is relatively high due to toluene has slight solubility in water[56], which resulted in relatively low separation efficiency (>91.5%). The permeability of the membrane was calculated by measuring the time needed to collect a certain volume of filtrate during the process of separating various oil/water emulsions. The fluxes for T/W, H/W, O/W, I/G, T80/T/W, S/O/W and S/I/W emulsions were 634, 688, 672, 644, 592, 603, 597 $Lm^{-2}h^{-1}$, respectively. Compared to the permeation performances of common commercial membrane (regenerated cellulose membrane C100F, Microdyne-Nadir GmbH)[57] (the flux for emulsion with an oil concentration of 0.5-1.5% is less than 200 $Lm^{-2}h^{-1}$ at 0.5-1.5 MPa under pH5-7), the flux results suggest the remarkable permeability of the membrane, considering no external pushing force used in the separation process.

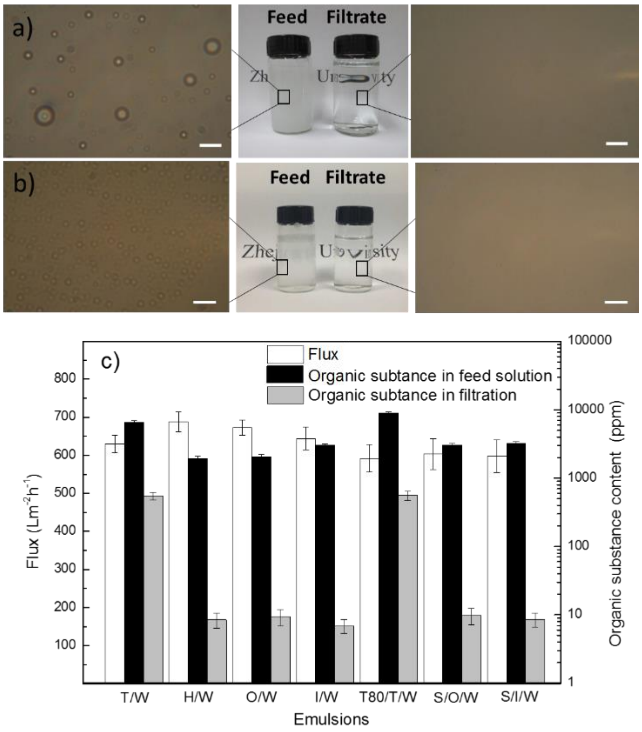

Figure 9. a-b) Separation results of the toluene/water emulsions and Tween80-stabilized toluene/water as examples; scale bar=10 µm. c) Separation performance for a series of oil/water emulsions.

In the treatment of oily wastewater, antifouling properties are very important. Because the NLGM shows ultralow affinity for oil droplets, we infer that it has excellent antifouling properties. Here, we took the SDS-stabilized isopar G/water emulsion as an example to test the NLGM antifouling properties because isopar G is an often-used solvent in industry and is composed of various types of isoparaffin. The separation of SDS-stabilized isopar G/water emulsion is similar to real conditions in practical industry applications. Figure 9 plots the recyclability using the SDS-stabilized isopar G-in-water emulsion. In every cycle, the membrane was rinsed with water after a certain amount of filtrate was collected. As shown in Figure 10, over 10 cycles, the membrane still maintained stable performance. The flux was nearly unchanged with increasing cycle time, indicating that the membrane has excellent antifouling properties. This result may be attributed to the ultralow adhesion of oil to the membrane surface, which was demonstrated by the SEM images of membrane surface after emulsion separation, as shown in Figure S5. We can see that the membrane surface almost unchanged and the integrity of the membrane structure maintained after repeatedly separation process. Hence as we expected, the wetting properties of the membrane was maintained as well. For example, the underwater oil droplet angle of the membrane is ~157° after SDS/isorpar G/water emulsion and the membrane surface still has low affinity to oil droplet (Figure S6). These results suggest the capability of the membrane for long-term use in the treatment of oil/water mixtures.

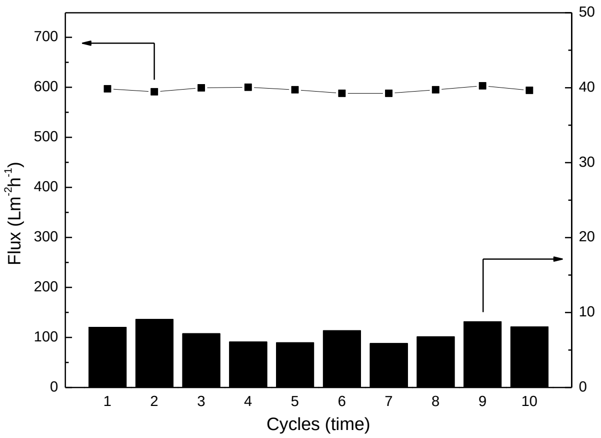

Figure 10. Cycling performance of the membrane using SDS-stabilized isopar G/water emulsion as the model system.

Conclusions

In summary, a novel non-laminated GO membrane crosslinked by polyethyleneimine (PEI) was prepared via a one-step sol-gel process. The merit of this method lies in its easy applicability, which is especially favorable for scaling-up in industry. Using various characterization techniques, it was proved that GO successfully reacted with PEI and that GO nanosheets in the membrane were randomly arranged, forming a sponge-like non-laminated microstructure. This special structure endows the membrane with a lower flow resistance compared with usual laminated GO membranes; therefore, a much higher flux was achieved. Further, combining the hydrophilic surface chemistry with the micro/nanoscale hierarchical surface structure, the membrane shows superhydrophilic and underwater superoleophobic properties, which can effectively separate a wide range of surfactant-free and surfactant stabilized undissolved oil-in-water emulsions with droplet sizes from the micrometer to the nanometer range. Using only gravity, a high separation efficiency (>99%) and fluxes were achieved. More significantly, due to the low affinity of this membrane to oil droplets in water, it shows excellent antifouling properties and is easy to recycle for long-term use. This work is the first study on non-laminated GO membranes, which may inspire future study on designing novel GO membranes for separation fields as well as many other applications.

Acknowledgements

The authors acknowledge financial support for this work from Zhejiang Provincial Natural Science Foundation of China (No.LR12B06001); the National Basic Research Program of China (2015CB655303); the National Natural Science Foundation of China (No. 20946003).

Notes and references

1 D. R. Dreyer, S. Park, C. W. Bielawski and R. S. Ruoff, *Chemical Society Reviews*, 2010, **39**, 228-240.
2 H. Bai, C. Li, X. L. Wang and G. Q. Shi, *Journal of Physical Chemistry C*, 2011, **115**, 5545-5551.
3 X. J. Zhu, Y. W. Zhu, S. Murali, M. D. Stollers and R. S. Ruoff, *ACS Nano*, 2011, **5**, 3333-3338.
4 Y. T. Chen, F. Guo, A. Jachak, S. P. Kim, D. Datta, J. Y. Liu, I. Kulaots, C. Vaslet, H. D. Jang, J. X. Huang, A. Kane, V. B. Shenoy and R. H. Hurt, *Nano Letters*, 2012, **12**, 1996-2002.
5 X. C. Dong, H. Xu, X. W. Wang, Y. X. Huang, M. B. Chan-Park, H. Zhang, L. H. Wang, W. Huang and P. Chen, *ACS Nano*, 2012, **6**, 3206-3213.
6 P. K. Santra and P. V. Kamat, *Journal of the American Chemical Society*, 2012, **134**, 2508-2511.
7 J. N. Tiwari, K. Nath, S. Kumar, R. N. Tiwari, K. C. Kemp, N. H. Le, D. H. Youn, J. S. Lee and K. S. Kim, *Nat. Commun.*, 2013, **4**, 7.
8 M. Z. Seyedin, J. M. Razal, P. C. Innis, R. Jalili and G. G. Wallace, *Advanced Functional Materials*, 2015, **25**, 94-104.
9 W. Li, J. S. Wang, J. S. Ren and X. G. Qu, *Advanced Materials*, 2013, **25**, 6737-6743.
10 D. A. Dikin, S. Stankovich, E. J. Zimney, R. D. Piner, G. H. B. Dommett, G. Evmenenko, S. T. Nguyen and R. S. Ruoff, *Nature*, 2007, **448**, 457-460.
11 X. W. Yang, L. Qiu, C. Cheng, Y. Z. Wu, Z. F. Ma and D. Li, *Angewandte Chemie-International Edition*, 2011, **50**, 7325-7328.
12 H. B. Huang, Z. G. Song, N. Wei, L. Shi, Y. Y. Mao, Y. L. Ying, L. W. Sun, Z. P. Xu and X. S. Peng, *Nat. Commun.*, 2013, **4**.
13 R. K. Joshi, P. Carbone, F. C. Wang, V. G. Kravets, Y. Su, I. V. Grigorieva, H. A. Wu, A. K. Geim and R. R. Nair, *Science*, 2014, **343**, 752-754.
14 B. X. Mi, *Science*, 2014, **343**, 740-742.
15 H. Y. Liu, H. T. Wang and X. W. Zhang, *Advanced Materials*, 2015, **27**, 249-254.
16 H. W. Kim, H. W. Yoon, S. M. Yoon, B. M. Yoo, B. K. Ahn, Y. H. Cho, H. J. Shin, H. Yang, U. Paik, S. Kwon, J. Y. Choi and H. B. Park, *Science*, 2013, **342**, 91-95.
17 H. Li, Z. N. Song, X. J. Zhang, Y. Huang, S. G. Li, Y. T. Mao, H. J. Ploehn, Y. Bao and M. Yu, *Science*, 2013, **342**, 95-98.
18 L. Qiu, X. H. Zhang, W. R. Yang, Y. F. Wang, G. P. Simon and D. Li, *Chem. Commun.*, 2011, **47**, 5810-5812.
19 R. R. Nair, H. A. Wu, P. N. Jayaram, I. V. Grigorieva and A. K. Geim, *Science*, 2012, **335**, 442-444.
20 Y. Han, Z. Xu and C. Gao, *Advanced Functional Materials*, 2013, **23**, 3693-3700.
21 K. Huang, G. P. Liu, Y. Y. Lou, Z. Y. Dong, J. Shen and W. Q. Jin, *Angewandte Chemie-International Edition*, 2014, **53**, 6929-6932.
22 N. V. Medhekar, A. Ramasubramaniam, R. S. Ruoff and V. B. Shenoy, *ACS Nano*, 2010, **4**, 2300-2306.
23 C. N. Yeh, K. Raidongia, J. J. Shao, Q. H. Yang and J. X. Huang, *Nat. Chem.*, 2015, **7**, 166-170.
24 24.S. Park, K. S. Lee, G. Bozoklu, W. Cai, S. T. Nguyen and R. S. Ruoff, *ACS Nano*, 2008, **2**, 572-578.
25 S. Park, D. A. Dikin, S. T. Nguyen and R. S. Ruoff, *Journal of Physical Chemistry C*, 2009, **113**, 15801-15804.
26 Z. An, O. C. Compton, K. W. Putz, L. C. Brinson and S. T. Nguyen, *Advanced Materials*, 2011, **23**, 3842-+.
27 M. Hu and B. X. Mi, *Environmental Science & Technology*, 2013, **47**, 3715-3723.
28 W. S. Hung, C. H. Tsou, M. De Guzman, Q. F. An, Y. L. Liu, Y. M. Zhang, C. C. Hu, K. R. Lee and J. Y. Lai, *Chemistry of Materials*, 2014, **26**, 2983-2990.
29 T. F. Huang, L. Zhang, H. L. Chen and C. J. Gao, *Journal of Materials Chemistry B*, 2015, **3**, 1605 - 1611.
30 Z. X. Xue, S. T. Wang, L. Lin, L. Chen, M. J. Liu, L. Feng and L. Jiang, *Advanced Materials*, 2011, **23**, 4270-4273.
31 M. L. Huang, Y. Si, X. M. Tang, Z. G. Zhu, B. Ding, L. F. Liu, G. Zheng, W. J. Luo and J. Y. Yu, *Journal of Materials Chemistry A*, 2013, **1**, 14071-14074.
32 F. Zhang, W. B. Zhang, Z. Shi, D. Wang, J. Jin and L. Jiang, *Advanced Materials*, 2013, **25**, 4192-4198.
33 W. B. Zhang, Z. Shi, F. Zhang, X. Liu, J. Jin and L. Jiang, *Advanced Materials*, 2013, **25**, 2071-2076.
34 X. Gao, L. P. Xu, Z. Xue, L. Feng, J. Peng, Y. Wen, S. Wang and X. Zhang, *Advnced Materials*, 2014, **26**, 1771-1775.
35 M. M. Tao, L. X. Xue, F. Liu and L. Jiang, *Advanced Materials*, 2014, **26**, 2943-2948.
36 W. B. Zhang, Y. Z. Zhu, X. Liu, D. Wang, J. Y. Li, L. Jiang and J. Jin, *Angewandte Chemie-International Edition*, 2014, **53**, 856-860.
37 S. Park, J. H. An, R. D. Piner, I. Jung, D. X. Yang, A. Velamakanni, S. T. Nguyen and R. S. Ruoff, *Chemistry of Materials*, 2008, **20**, 6592-6594.
38 T. Szabo, O. Berkesi, P. Forgo, K. Josepovits, Y. Sanakis, D. Petridis and I. Dekany, *Chemistry of Materials*, 2006, **18**, 2740-2749.
39 D. Yang, A. Velamakanni, G. Bozoklu, S. Park, M. Stoller, R. D. Piner, S. Stankovich, I. Jung, D. A. Field, C. A. Ventrice and R. S. Ruoff, *Carbon*, 2009, **47**, 145-152.
40 H. L. Ma, H. B. Zhang, Q. H. Hu, W. J. Li, Z. G. Jiang, Z. Z. Yu and A. Dasari, *Acs Applied Materials & Interfaces*, 2012, **4**, 1948-1953.
41 S. Stankovich, D. A. Dikin, R. D. Piner, K. A. Kohlhaas, A. Kleinhammes, Y. Jia, Y. Wu, S. T. Nguyen and R. S. Ruoff, Carbon, 2007, **45**, 1558-1565.
42 M. X. Chen, C. C. Zhang, X. C. Li, L. Zhang, Y. L. Ma, L. Zhang, X. Y. Xu, F. L. Xia, W. Wang and J. P. Gao, Journal of Materials Chemistry A, 2013, **1**, 2869-2877.

43 Z. Tang, S. Shen, J. Zhuang and X. Wang, *Angewandte Chemie-International Edition*, 2010, **49**, 4603-4607.
44 Y. X. Xu, K. X. Sheng, C. Li and G. Q. Shi, *ACS Nano*, 2010, **4**, 4324-4330.
45 X. Zhang, Z. Sui, B. Xu, S. Yue, Y. Luo, W. Zhan and B. Liu, *J. Mater. Chem.*, 2011, **21**, 6494-6497.
46 R. L. D. Whitby, A. Korobeinyk, V. M. Gun'ko, R. Busquets, A. B. Cundy, K. Laszlo, J. Skubiszewska-Zieba, R. Leboda, E. Tombacz, I. Y. Toth, K. Kovacs and S. V. Mikhalovsky, *Chem. Commun.*, 2011, **47**, 9645-9647.
47 S. Ansari and E. P. Giannelis, *Journal of Polymer Science Part B-Polymer Physics*, 2009, **47**, 888-897.
48 R. L. D. Whitby, A. Korobeinyk, S. V. Mikhalovsky, T. Fukuda and T. Maekawa, *Journal of Nanoparticle Research*, 2011, **13**, 4829-4837.
49 S. Xie, X. Liu, B. Zhang, H. Ma, C. Ling, M. Yu, L. Li and J. Li, *Journal of Materials Chemistry A*, 2015, **3**, 2552-2558.
50 H. Hu, Z. Zhao, W. Wan, Y. Gogotsi and J. Qiu, *Advanced Materials*, 2013, **25**, 2219-2223.
51 N. Zhang, H. Qiu, Y. Si, W. Wang and J. Gao, *Carbon*, 2011, **49**, 827-837.
52 M. Chen, C. Zhang, X. Li, L. Zhang, Y. Ma, L. Zhang, X. Xu, F. Xia, W. Wang and J. Gao, *Journal of Materials Chemistry A*, 2013, **1**, 2869-2877.
53 N. Li, Q. Zhang, S. Gao, Q. Song, R. Huang, L. Wang, L. Liu, J. Dai, M. Tang and G. Cheng, *Sci Rep*, 2013, **3**, 1604.
54 A. Tuteja, W. Choi, M. L. Ma, J. M. Mabry, S. A. Mazzella, G. C. Rutledge, G. H. McKinley and R. E. Cohen, *Science*, 2007, **318**, 1618-1622.
55 A. B. D. Cassie, *Discussions of the Faraday Society*, 1948, **3**, 11-16.
56 H. Stephen and T. Stephen, Solubilities of inorganic and organic compounds, Pergamon Press, Oxford, 1979, Vol. 1: Binary systems, Part 1, pp 67.
57 M. Hesampour, A. Krzyzaniak and M. Nystrom, Journal of Membrane Science, 2008, **325**, 199-208.